

Concept-free Causal Disentanglement with Variational Graph Auto-Encoder

Jingyun Feng¹ Lin Zhang² Lili Yang¹

Abstract

In disentangled representation learning, the goal is to achieve a compact representation that consists of all interpretable generative factors in the observational data. Learning disentangled representations for graphs becomes increasingly important as graph data rapidly grows. Existing approaches often rely on Variational Auto-Encoder (VAE) or its causal structure learning-based refinement, which suffer from sub-optimality in VAEs due to the independence factor assumption and unavailability of concept labels, respectively. In this paper, we propose an unsupervised solution, dubbed concept-free causal disentanglement, built on a theoretically provable tight upper bound approximating the optimal factor. This results in an SCM-like causal structure modeling that directly learns concept structures from data. Based on this idea, we propose Concept-free Causal VGAE (CCVGAE) by incorporating a novel causal disentanglement layer into Variational Graph Auto-Encoder. Furthermore, we prove concept consistency under our concept-free causal disentanglement framework, hence employing it to enhance the meta-learning framework, called concept-free causal Meta-Graph (CC-Meta-Graph). We conduct extensive experiments to demonstrate the superiority of the proposed models: CCVGAE and CC-Meta-Graph, reaching up to 29% and 11% absolute improvements over baselines in terms of AUC, respectively.

1. Introduction

Graph data becomes ubiquitous, in both natural and human-made scenarios, along with the rise of deep learning, gaining increasing attention and making learning on graphs an emerging research field, with the goal of understanding graphs and dealing with downstream applications, such as

¹Department of Statistics and Data Science, Southern University of Science and Technology, Shenzhen, Guangdong, China.
²Gongsheng Matrix, Shenzhen, China.

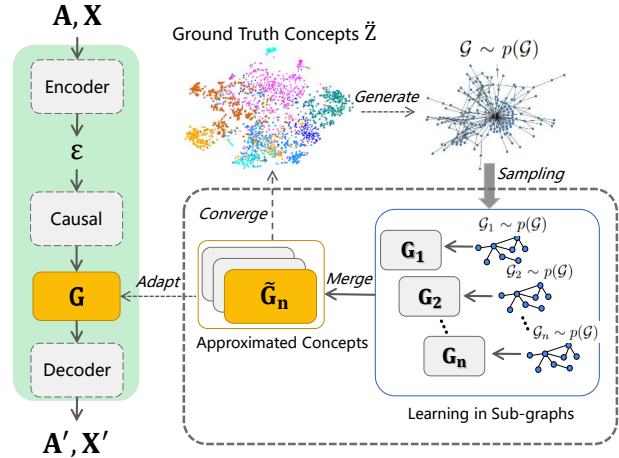


Figure 1. An illustration of our proposed ideas. The left component (shown in light green) demonstrates a causal disentanglement process in a single graph, i.e., CCVGAE which takes an adjacency matrix and node features as inputs. The right-hand component shows the consistency property of generative factors obtained by CCVGAE. This property implies that merging generative factors from other graphs can be adapted to others, and thus leads to an extension of CCVGAE, called CC-Meta-Graph. Here, we assume all graphs are sampled from the same graph (i.e., \mathcal{G}). \tilde{G}_n represents the approximated concepts by merging the individual concepts (G_i) obtained from the samples (\mathcal{G}_i).

drug discovery (You et al., 2018), traffic forecasting (Jiang & Luo, 2022), recommender systems (Wu et al., 2020), and others (Zhou et al., 2020). Of particular importance is graph representation learning (Hamilton, 2020), but it remains an outstanding research problem due to graphs’ non-IID and non-Euclidean properties. There is growing attention to the disentanglement learning to address this problem.

The goal of disentanglement learning is to acquire the representations that capture all interpretable generative factors, called disentangled representations (Bengio et al., 2013; Higgins et al., 2018). A significant challenge of disentanglement learning is that we often only have raw observations while not allowing any supervision on generative factors (i.e., causes) (Kumar et al., 2017). Earlier attempts (Paige et al., 2017; Yang et al., 2021) often demand adequate labels for training and hence can not fit the above realistic setting. This motivates us to focus on the unsupervised

setting. Recent advances in unsupervised disentanglement learning have mostly focused on Variational Auto-encoders (VAEs) (Li & Mandt, 2018) and Generative Adversarial Networks (GANs) (Kocaoglu et al., 2017). In particular, the VAE framework is preferred in graphs because of its stability in contrast to mode collapse in GANs due to its implicit modeling of the distribution, which is especially difficult to learn the distribution of graphs. So in this work, our focus is on the VAE framework to explore disentanglement for graph representation learning, i.e., Variational Graph Auto-Encoders (VGAE) (Kipf & Welling, 2016a).

Despite the recent growth of disentanglement learning, most state-of-the-art methods within the VAE framework have assumed that the distributions in the hidden space are independent Gaussian (Kim & Mnih, 2018) and thus lead to suboptimal solutions (Träuble et al., 2021). Studies (Locatello et al., 2020; Trauble et al., 2020) have shown that disentanglement of representations is nearly impossible under the independent assumption when the data demonstrates intrinsic correlations. In contrast, modeling the structure for underlying factors enhances disentanglement, particularly causal structure learning (Schölkopf & von Kügelgen, 2022). However, when leveraging the VAE framework, there is no adequate research on the optimal solution while imposing a causal structure on the latent factors.

In this paper, we attempt to address unsupervised causal disentangled representation learning in the VGAE framework, including theoretical analysis and practical methodologies. We prove a tight upper bound on approximating the optimal latent factor via causal structure learning. It indicates that a linear causal modeling function can approximate the optimal latent factor with high confidence. With this, we then develop a practical causal disentanglement method without requiring concept labels, called concept-free causal disentanglement. In this way, we achieve a data-driven causal structure modeling that directly learns concept structures from data. Building on this, we introduce a novel causal disentanglement layer and then integrate it with VGAE, resulting in our first model, called Concept-free Causal VGAE (CCVAGE). Besides, we uncover the consistency of our obtained concepts due to the data-driven style, making them suitable for capturing underlying global information with little data. Towards this, we propose a meta-learning model that transfers global-aware concepts to newly arrived data, resulting in our second model, called CC-Meta-Graph. In Figure 1, we present an illustration of the proposed ideas.

We highlight the contributions of this paper:

- 1, In this paper, we theoretically prove a tight bound on the approximation of optimal factors and offer a practical causal disentanglement method on top of it, called concept-free causal disentanglement.
- 2, We propose two causal disentanglement-enhanced mod-

els: one is to support causal disentanglement in VGAE, and the other is to validate the proposed consistency property.

- 3, We conduct extensive experiments with synthetic and real-world graph data to demonstrate the efficiency of our proposed models in terms of link prediction, achieving up to 29% and 11% absolute improvements for CCVGAE and CC-Meta-Graph, respectively.¹

2. Related work

Disentanglement Learning. The concept of disentanglement was first introduced by Bengio et al. (2013) as a property of representation and its formal definition Higgins et al. (2018) is: if a representation can be decomposed into several independent features, which means only one of these features will change when change one factor of data input, then we call it "*disentangled representation*". Some studies (Eastwood & Williams, 2018) consider a more rigorous definition that only if each dimension of the representation can capture at most one true generative factor, we can call this representation a "*disentangle representation*". In order to encourage potential factors to learn disentangled representations while optimizing the inherent task objectives, disentangled representation learning is designed to capture interpretable, controllable and robust representations.

In graph disentangled representation learning, most frameworks are GNN-based. DisenGCN (Ma et al., 2019) utilizes neighbourhood routing to identify the latent factor that may caused edges, FactorGCN (Yang et al., 2020) disentangle graph into several sub-graphs, each sub-graph represent graph composed of one type of edges. However, Fan et al. (2022) noticed that GNNs always suffer from spurious correlation, even if the causal correlation always exists. They proposed DisC to learn causal substructure and bias substructure. DisC requires some of input graph nodes represent concepts. However, such graphs are always unavailable in real world.

Most typical disentangled representation learning methods are generative models, especially Variational Auto-Encoder(VAE) (Higgins et al., 2016; Kumar et al., 2017; Yang et al., 2021; Zhu et al., 2021). VAE use a variational posterior $q(z|x)$ to approximate the unknown true posterior $p(z|x)$. To obtain better disentanglement ability, researchers design various extra regularizers based on the original VAE loss function. A penalty coefficient is introduced to ELBO loss by β -vae (Higgins et al., 2016) to strengthen the independence constraint of the variational posterior distribution $q(z|x)$. FactorVAE (Kim & Mnih, 2018) imposes independence constraint according to the definition of independence. However, better disentanglement ability often leads to more

¹The experiments code can be found in <https://www.dropbox.com/sh/c8nd1qbp20ling/AABhhjr1RGOF4X5h-oswoaza?dl=0>

reconstruction errors. To balance the trade-off between reconstruction and disentanglement, Burgess et al. (2018) proposes a simple modification based on β -VAE, making the quality of disentanglement can be improved as much as possible without too much reconstruction error. However, we believe that the conflict between reconstruction error and disentanglement quality does not naturally exist but from the improper disentanglement such as independent assumption as follows. Higgins et al. (2018) assumed that the generating factors were natural and independent in disentangled representation learning.

However, Suter et al. (2019) disagreed with the independence assumption. They assumed that the generating factors of the observable data are causally influenced by the group of confounding factors, and first introduced SCM (Kraewski & Matthews, 2010) to describe causal relationships among generating factors. Träuble et al. (2021) suggested that, if some generating factors are correlated in the data set, methods based on independent assumption might have a bias against disentanglement. Other researchers (Yang et al., 2021; Shen et al., 2022) have also taken experiments of disentanglement learning in real-world data based on the assumption that the real-world data is not generated by independent factors. Here, we also follow the same assumption that generates factors are not independent and even believe there are underlining causal relationships among these factors.

Causal Disentanglement. Over the past decades, many researchers (Hoyer et al., 2008; Zhang & Hyvarinen, 2012; Shimizu et al., 2006) have paid attention to the discovery of causality from observational data. With the development of disentanglement learning, the community has raised the interest in combining causality and disentangled representation. Kocaoglu et al. (2017) proposed a method called CausalGAN which supports "do-operation" on images but it requires the causal graph given as a prior. Suter et al. (2019) believed that the underlying causal generative process will impact the level of disentanglement, and firstly proposed the definition of the causal disentanglement process.

Yang et al. (2021) is the first to implement the causal disentanglement process proposed by Suter et al. (2019), called CausalVAE. However, their method is semi-supervised because they require labels of generative factors. But such labels are uneasily acquired in the graph, so our work concentrates on an unsupervised method, which makes latent variables learn underlying causal information from data.

3. Notations and Preliminaries

Notations. Formally, let $\mathcal{G} = (\mathcal{V}, \mathcal{E})$ denotes an undirected and unweighted graph, with its adjacency matrix and degree matrices as $Adj = \{0, 1\}^{n \times n}$ and D , respectively. Here, \mathcal{V}

and \mathcal{E} are the node and edge sets, where $n = |\mathcal{V}|$. Nodes are associated with pre-defined attributes, written as $Attri \in \mathbb{R}^n$. We use $\mathcal{N}(\cdot)$ to represent Gaussian distribution.

Variational Graph Auto-Encoder (VGAE). In VGAE, the high-dimensional observation ε is projected into a low-dimensional space for compact representation z using an encoder-decoder framework. Concretely, the encoder compresses the input data, and the decoder checks the soundness of the compressed one by recovering raw data. Mathematically, we often optimize VAE by maximizing evidence lower bound (ELBO), denoting as $\max_{p,q} \mathcal{L}_{VAE}(\varepsilon)$, where $\mathcal{L}_{VAE}(\varepsilon) = \mathbb{E}_{q(z|\varepsilon)}[\log p(\varepsilon | z)] - D_{KL}(q(z | \varepsilon) || p(z))$, where D_{KL} is the Kullback-Leibler divergence (Joyce, 2011). **VGAE is a special cases of VAE**, with graph-based functions for $q(\cdot)$ and $p(\cdot)$. Using graph convolutional network (GCN) (Zhang et al., 2018), we have them defined as follows: $p(Adj_{ij} = 1 | \varepsilon_i, \varepsilon_j) = \sigma(\varepsilon_i^\top \varepsilon_j)$ and $q(\varepsilon_i | Adj, Attri) = N(\mu_i, diag(\sigma_i))$, where the mean is $\mu = GCN_\mu(Adj, Attri)$ and covariance is $\sigma = GCN_\sigma(Adj, Attri)$. Here, $\sigma(\cdot)$ is an activation function and takes the logistic Sigmoid function by default.

Linear Structured Causal Model (SCM). Linear SCM defines a causal system with linear equations representing the semantics as follows (Shimizu et al., 2006; Yang et al., 2021), with independent exogenous factors $\epsilon \in \mathbb{R}^K$ and endogenous variables $z \in \mathbb{R}^K$,

$$z = \Phi^T z + \epsilon = (I - \Phi^T)^{-1} \epsilon, \epsilon \sim \mathcal{N}(0, I) \quad (1)$$

where $\Phi \in \mathbb{R}^{K \times K}$ is an adjacency matrix for a directed acyclic graph (DAG) that captures the causal structure of n concepts. *Note we use the same letters here to avoid the abuse of notation.*

Disentangled Causal Process (DCP). DCP studies disentanglement in the latent space by considering confounding variables, which results in theoretically sound properties as opposed to heuristics in the prior (Suter et al., 2019). Its detailed definition is as follows.

Definition 3.1. *Given m causal generative factors as $G = [G_1, \dots, G_m]$ and L confounders as $C = \{C_1, \dots, C_L\}$, causal disentanglement for the observation X is possible if and only if X can be represented in a SCM context as follows,*

$$C \leftarrow \zeta_C \quad (2)$$

$$G_i \leftarrow q_i(H_i^C, \zeta_i), i = 1, 2, \dots, m \quad (3)$$

$$X \leftarrow g(G, \zeta_x) \quad (4)$$

Here, $H_i^C \in \{C_1, \dots, C_L\}$ is the father node of G_i , i.e., $H_i^C \rightarrow G_i$ holds regarding causality. $\zeta_c, \{\zeta_i\}_{i=1,2,\dots,m}, \zeta_x$ are independent noise variables. Note q_i and g are pre-defined functions.

4. Theory

In this section, we first formulate the problem of causal disentangled representation learning in VGAE. We next present a theoretical analysis of causal disentanglement, where we provide a tight upper bound to approximate the optimum (see Section 4.1). After that, we introduce a practical solution to accomplish this approximation together with its properties (see Section 4.2).

Problem Formulation. Denote the input graph data as X and its optimal latent factor as Z^* (Träuble et al., 2021), the optimal data distribution is formulated as $p^*(X) = \int_{Z^*} p^*(X|Z^*)p^*(Z^*)dZ^*$, along with an non-i.i.d. assumption on Z^* , i.e., $p^*(Z^*) \neq \prod_i p(Z_i^*)$. As a common solution to disentanglement, VGAE disentangles input data into latent representation Z , and the corresponding data distribution is $p_\theta(X) = \int_Z p_\theta(X|Z)p(Z)dZ$, where θ is the learnable parameters. Given that all correlations can be modeled as causal structures (Schölkopf & von Kügelgen, 2022), we let Z possess a causal structure and define this structure with DCP. Having no labels from Z , the goal of unsupervised causal disentangled representation learning in VGAE is to achieve an optimal latent factor Z^* while making $p_\theta(X) = p^*(X)$ always hold.

4.1. A theoretical analysis of causal disentanglement

Definition 4.1. Given the the process (2) and (3) in the DCP, we obtain the generative factors as $G = Q(\zeta^+)$, with $\zeta_G = \{\zeta_1, \zeta_2, \dots, \zeta_m\}$ and $\zeta^+ = \zeta_C \cup \zeta_G$. The distribution of data can be attained as $p_{\theta_{\zeta_x}}(X) = \int_G p_{\theta_{\zeta_x}}(X|G)p(G)dG$.

This definition suggests that a given data can be represented with causal generative factors while having no assumption of independence as in the previous VAE. Based on this, as we will see in Theorem 4.1, the causal disentanglement guarantees an optimal solution to attain the following: 1) the distribution consistency between the input data and the predicted one, i.e., $p_\theta(X) = p^*(X)$, and 2) the optimal latent factor Z^* . In contrast, traditional VAE imposes an independence assumption on Z and suffers a sub-optimality solution (Träuble et al., 2021) w.r.t the true data distribution, leading to $p_\theta(X) \neq p^*(X)$. With this difference, the above causal disentanglement avoids such a assumption.

Theorem 4.1. Given independent Normal distributed variables $N = N_1, \dots, N_K$, there exists an optimal causality modeling function Q that represents the causal generative factor $G = \{G_1, \dots, G_K\} = Q(N)$, equating to the optimal disentangled latent factor Z^* , while holding $p_{\theta_{\zeta_x}}(X) = p^*(X)$.

We defer the proof of Theorem 4.1 to the Appendix A.1. Theorem 4.1 proves that in a casual setting, there must **exist an optimal solution** for the VAE. Next, we introduce a generalized causal generative factor expression that unifies

the base for causal disentanglement.

Definition 4.2. (general causal generative factor expression). Given independent Normal distributed variables $N = \{N_1, \dots, N_K\}$ and a matrix $A \in \mathbb{R}^{K \times K}$, any causal generative factor can be formulated as $G_i = Q_i(B_i)$, where $B = A * \text{diag}(N)$.

According to Theorem 4.1 and the above definition, we attain a **unified optimal expression** of generative factor as follows (detailed proof is at Appendix A.2):

Proposition 1. (unified optimal generative factor expression). Let A as a lower triangular matrix, then the expression of optimal generative factors can be unified as $G_i = Q_i(B_i)$, where $B = \hat{A} * \text{diag}(N)$ and \hat{A} is permuted from A .

Having established the connections between optimal generative factors in Proposition 1, we arrive at a necessary condition for optimal factors. Whereas in this paper we aim to acquire both the necessary and sufficient conditions for the optimal factors. Solving these two together yields an analytical solution for the optimal factors (at Appendix A.1), making the implementation difficult in modern deep architectures. Such a solution becomes infeasible alongside an unknown distribution for the optimal latent representations. A practical solution is to **approximate the optimal factors**, within acceptable confidence, while being practically feasible.

Provided a representation base B_i , assume the existence of an approximated generative factor to the optimal one, $Q_i(B_i)$, over the same space, denoted as $Q'_i(B_i)$. We derive a tight upper bound on the approximation error by setting Q'_i as a linear function, as shown in Theorem 4.2.

Theorem 4.2. Given B_i in Proposition 1, and N_i with an interval of $N_i \in [\mu_i - \delta, \mu_i + \delta]$, $i = 1, 2, \dots, K$, for an optimal $Q_i(B_i)$, there exist a linear function Q'_i make $Q'_i(B_i)$, the absolute error has such bond: $|Q_i(B_i) - Q'_i(B_i)| \leq O_i(\delta)$, where $O_i(\delta) = a_i + \delta \Lambda_i$, $\Lambda_i = b_i + \sum_{t=1}^i c_{it} d_t^{\delta^2}$, a_i, b_i, c_{it}, d_t are constant unrelated to δ , $0 < d_t < 1$, $i = 1, 2, \dots, K$ and $t = 1, 2, \dots, K$, δ is a non-negative real number unrelated to distribution of N .

Please see Appendix A.3 for more details. Theorem 4.2 suggests that over 95% probability, the range of N_i is within $[\mu_i - 2\sigma_i, \mu_i + 2\sigma_i]$ and hence the error is bound by $O_i(2\sigma_i)$, i.e., the bound is nearly constant with 95% confidence. Note that we assume the optimal latent representation $(Z_1^*, Z_2^*, \dots, Z_K^*)$ as a linear uniform distribution. One could arrive at different bounds with distributions, and we take the uniform distribution for simplicity.

4.2. Concept-free Causal Disentanglement

Theorem 4.2 says we can obtain an approximated optimal generative factor by appointing the projection function linear. This approximation enables a practical implementation toward the optimal latent factor. Formally, we introduce the linear projection-based generative factor:

Proposition 2. (*Approximated generative factor expression*). Given independent Normal distributed variables $N = \{N_1, \dots, N_K\}$, a lower triangular matrix \tilde{A}_i , a causal generative factor can be formulated as $G'_i = Q'_i(B_i) = \tilde{A}_i * N'$, where \tilde{A} is obtained by permuting a lower triangular matrix.

The proof is given in the Appendix A.4. We set our causal disentanglement in the context of the Structural Causal Model (SCM) and focus on a linear SCM because of its simplicity. Following this, we formalize the causal structure in G as follows,

$$G' = \Phi G' + \varepsilon \rightarrow G' = (I - \Phi)^{-1} \varepsilon^T \quad (5)$$

where $\Phi \in \mathbb{R}^{K \times K}$ is a DAG adjacency matrix and ε is a independent variable. The resulting $(I - \Phi)^{-1}$ is also a permuted low triangular matrix, see the proof in Appendix A.6. Note that Proposition 2 is for a general causal setting. Letting $N = \varepsilon$, the above linear representation based on SCM shares the same expression as that in the proposition, and thus inherits the ideal property of approximating the optimal latent factor Z^* . Furthermore, the two variables in Eq. 5 are learned from data in a straightforward manner, without any labels for supervision. Denoted each G_i as a concept (Kumar et al., 2017) we arrive at an unsupervised causal disentanglement that does not require any concept labels, called concept-free causal disentanglement.

In unsupervised disentanglement learning, along with the linear Gaussian assumption, the identifiability problem (Locatello et al., 2019) often arises due to the discrepancy between the pre-defined concepts and the learned ones. Without supervision, we cannot achieve these pre-defined concepts, especially given limited data. However, as we will see in the following theorem, these pre-defined concepts are attainable when sufficient data is accessed. Since these concepts hold in multiple samples, making them the ground truth.

Theorem 4.3. Given n observations $\{X^{(1)}, X^{(2)}, \dots, X^{(n)}\}$ sampled from the same distribution $p^*(X)$, along with their corresponding optimal generative factors $\{Z^{(1)}, Z^{(2)}, \dots, Z^{(n)}\}$, the function of these generative factors will converge to the same ground truth (GT) concept.

A formal version of Theorem 4.3 and its proof can be found at Appendix A.5. More importantly, we believe concepts obtained by the theorem are better than human-labeled

concepts because these are limited and may involve bias. The above discrepancy does not always imply errors in the learned concepts, and conversely, the latter can be a compensation for human-defined ones.

Besides, Theorem 4.3 enables guaranteed learning toward the ground truth (GT) concepts and leads to the following property:

Property 1. (Consistency of generative factors). Given observations sampled from the same distribution, each sample’s optimal generative factors, i.e., Z^* , capture a portion of GT concepts, implying that one can approximate the GT concepts with a merging of Z^* , where we call the merged one an approximated concept.

The consistency property implies that concepts learned from individual samples capture the GT concepts shared by all data from the same distribution, making these concepts adaptable. Therefore, under the same distribution, transferring concepts from observed data to newly sampled data benefits the learning of new data, thus significantly reducing the data demand and avoiding training from scratch.

5. Method

In this section, we propose a novel VGAE with a causal disentanglement model, namely Concept-free Causal VGAE (CCVGAE), whose goal is to obtain optimal disentangled latent representations. We also introduce a concept-free causal disentanglement framework in a meta-learning setting, called concept-free causal Meta-Graph (CC-Meta-Graph), to harness the property of concept consistency. We begin by introducing the definition of CCVGAE as follows,

Definition 5.1. (CCVGAE). Given an input graph’s adjacency matrix Adj and node attributes $Attri$, the proposed CCVGAE is defined by:

- A prior data distribution $p^*(Z^*) \neq \prod_i p(Z_i^*)$ roots on a set of causal structured latent factors $Z^* = \{Z_1^*, Z_2^*, \dots, Z_K^*\}$.
- An encoder is composed of a GNN-based compression component and a causal disentanglement component. The former employs GNN to compress the adjacency matrix Adj and node attributes $Attri$ into a low-dimensional latent space as ϵ . The latter (parameterized by ϕ) performs our concept-free causal disentanglement with ϵ as input, optimizes the underlying causal structure Φ in the learning procedure, and outputs the posterior approximation parameters: $q_\phi(G' | \epsilon, \Phi)$ (see Eq. 5).
- A decoder $p_\psi(Adj | G')$ that takes the obtained latent factor Z to infer the adjacency matrix of the

input graph data and is parameterized by ψ , i.e., $p(\text{Adj}_{ij} = 1 \mid G_i, G_j) = \sigma(G_i^\top G_j)$, where $\sigma(\cdot)$ is the logistic sigmoid function.

Optimization Objective. The optimization of CCVGAE is to encourage an equivalence between the approximated distribution $p_{\theta_G}(X)$ and the optimal one $p^*(X)$. In particular, the evidence lower bound (ELBO) is used to minimize the divergence between the above two distributions, and to enforce that the distribution of ε is independent Gaussian, as follows,

$$\begin{aligned} \mathcal{L}_G &= E_{q(\hat{G}|\text{Adj}, \text{Attri})} \log(p(\text{Adj}|\hat{G})) + \\ &KL(q(\varepsilon|(\text{Adj}, \text{Attri})|N(0, I)). \end{aligned} \quad (6)$$

Apart from minimizing distribution divergences, we also want to shorten the distance between the observation and the recovered one by measuring the mean squared error (MSE), written as: $\mathcal{L}_{MSE} = MSE(\text{Attri}, p(\text{Attri}|\hat{G}))$.

Meanwhile, performing causal structure modeling demands a DAG constraint on Φ . For the convenience of optimization, we impose a differentiable constraint function (Yu et al., 2019) as: $\mathcal{L}_\Phi = \text{tr}((I - \frac{r}{K}\Phi \circ \Phi)^K) - K$, where r is an arbitrary positive number, $\text{tr}(\cdot)$ denotes trace norm and K denotes the number of concepts. Combining the above loss functions, we derive the overall loss function as follows,

$$\mathcal{L} = -\mathcal{L}_G + \alpha\mathcal{L}_\Phi + \beta\mathcal{L}_{MSE}, \quad (7)$$

where α and β are hyper-parameters. *The overall algorithm is in Appendix A.7.*

5.1. Concept-free Causal disentanglement Meta-graph

Meta-Graph (Bose et al., 2019) deals with the few-shot link prediction task: it aims to predict links on target graphs (\mathcal{G}_T) with a model trained on a few source graphs (\mathcal{G}_S), where the source and target graphs are drawn from the same domain. Denoted the distribution over graphs in the same domain as $p(\mathcal{G})$, the distributions of the source and target graphs follow the same, i.e., $\mathcal{G}_S \sim p(\mathcal{G})$ and $\mathcal{G}_T \sim p(\mathcal{G})$. To accomplish this task, we demand high-quality adaptation that transfers the information in the training data to newly arrived data.

According to Property 1, our concept-free causal disentanglement can provide fast adaptation and hence is well suited for a meta-learning setting. Meta-Graph employs traditional VGAE to capture information to supply an initialization for training a subsequent link prediction model. Thanks to the consistency property, our proposed disentanglement solution can capture information (i.e., concepts) that is adaptable to newly arrived data. To this end, we replace VGAE with CCVGAE and let the other components remain in the Meta-Graph, called CC-Meta-Graph. *We present the corresponding algorithm in Appendix A.7.*

6. Experiments

6.1. Task 1: Link Prediction

This experiment aims to study how the proposed method, CCVGAE, performs on the link prediction task when compared to state-of-the-art methods.

Datasets. We experiment on 6 graph benchmark datasets from various domains (Sen et al., 2008; Pei et al., 2020; Tang et al., 2009), including Cora, dRisk, Actor, Corn, Texas, and Wisconsin. Table 6.1 presents the statistics of these datasets, including the numbers of nodes, edges, and node attributes.

Table 1. Statistics of datasets in our experiments. Note the initial number of edges for the synthetic data is 4894. # demotes number of.

Dataset	# Node	# Edge	# Attr
Cora	2708	5429	1433
Corn	183	295	1703
Texas	183	309	1703
Wisconsin	251	499	1703
dRisk	100	478	4
Actor	7600	33544	931
Synthetic	100	4984*	16

Note that dRisk is a data set transformed from dRiskKB (Xu et al., 2014), constructed from the biological text. dRiskKB contains 12981 nodes representing disease names, with weighted edges indicating correlations between disease pairs. To simplify the dataset, we randomly select 100 nodes from dRiskKB and transfer the weighted edges to the non-weighted edges. The dRiskKB does not provide node attributes, so we randomly generate 4 dimensions of one-hot features as node attributes.

Considering that real-world datasets often have unknown causality, we thus construct synthetic data with controllable causality. In particular, we produce attributes of nodes, X , and the adjacency matrix, $\text{Adj} \in \mathbb{R}^{100 \times 100}$, as follows: $\text{Adj} = \sigma(Z \cdot Z^T)$ and $\text{Attri} = 20\text{Sin}(Z)$. Here, we produce Z using linear SCM to ensure its causality. Mathematically, we derive $Z = C^T Z + \varepsilon \rightarrow Z = (I - C^T)^{-1}\varepsilon$, where $C \in \mathbb{R}^{16 \times 16}$ is a random lower triangular matrix and $\varepsilon \in \mathbb{R}^{16}$ is an independent random vector with same variance normal distribution.

Baselines. We compare CCVGAE to three prior methods: (1) VGAE (Kipf & Welling, 2016b), which is the first graph-based VAEs; (2) SIG-VAE (Hasanzadeh et al., 2019), which uses a hierarchical variational framework for encoder and a Bernoulli-Poisson link decoder; (3) DGAE (Wu & Cheng, 2022) incorporates standard auto-encoders (AEs) into GAEs to enhance the ability of modeling structured information.

Metrics. To evaluate our method, we perform the link prediction task and thus take two commonly used metrics

Table 2. AUC (%) and AP (%) scores for all baselines on real-world datasets. Note that X-DGAE shows the best results among all variations of DGAE, including 6-DGAE $_{\alpha}^{\beta}$, 36-DGAE $_{\alpha}^{\beta}$, and 64-DGAE $_{\alpha}^{\beta}$. * denotes results from the original article.

	GVAE		SIG-VAE		X-DGAE		CCVGAE		CCVGAE w/o CC	
	AUC	AP	AUC	AP	AUC	AP	AUC	AP	AUC	AP
Cora	0.91 \pm 0.02	0.92 \pm 0.01	0.92 \pm 0.01	0.93 \pm 0.02	0.93 \pm 0.02	0.92 \pm 0.02	0.85 \pm 0.03	0.85 \pm 0.05	0.72 \pm 0.04	0.73 \pm 0.03
Corn	0.53 \pm 0.03	0.66 \pm 0.06	0.62 \pm 0.05	0.64 \pm 0.03	0.73 \pm 0.10	0.77 \pm 0.10	0.74 \pm 0.06	0.78 \pm 0.04	0.68 \pm 0.06	0.73 \pm 0.05
Texas	0.51 \pm 0.06	0.59 \pm 0.04	0.60 \pm 0.03	0.63 \pm 0.05	0.46* \pm 0.09	0.61* \pm 0.08	0.75 \pm 0.07	0.80 \pm 0.07	0.74 \pm 0.05	0.75 \pm 0.06
Wisconsin	0.57 \pm 0.04	0.68 \pm 0.04	0.68 \pm 0.05	0.69 \pm 0.06	0.54* \pm 0.09	0.67* \pm 0.09	0.75 \pm 0.04	0.79 \pm 0.05	0.68 \pm 0.04	0.69 \pm 0.04
dRisk	0.61 \pm 0.03	0.62 \pm 0.05	0.58 \pm 0.03	0.56 \pm 0.04	0.73 \pm 0.11	0.72 \pm 0.10	0.75 \pm 0.06	0.72 \pm 0.05	0.63 \pm 0.05	0.62 \pm 0.06
Actor	0.76 \pm 0.07	0.81 \pm 0.06	0.77 \pm 0.03	0.80 \pm 0.05	0.77 \pm 0.02	0.80 \pm 0.03	0.78 \pm 0.07	0.81 \pm 0.06	0.72 \pm 0.03	0.76 \pm 0.04

Table 3. The performance of Meta-Graph-based baselines under different settings: varying number of meta-training loops and the requirement of meta-training data.

loops	PPI						FIRSTMM_DB					
	CC-Meta-Graph		Meta-Graph		Rand-Meta-Graph		CC-Meta-Graph		Meta-Graph		Rand-Meta-Graph	
	5%	10%	5%	10%	5%	10%	5%	10%	5%	10%	5%	10%
10	0.70 \pm 0.01	0.76 \pm 0.01	0.59 \pm 0.02	0.70 \pm 0.01	0.50 \pm 0.01	0.50 \pm 0.00	0.59 \pm 0.02	0.61 \pm 0.01	0.57 \pm 0.01	0.59 \pm 0.01	0.50 \pm 0.01	0.50 \pm 0.01
30	0.70 \pm 0.01	0.77 \pm 0.01	0.66 \pm 0.01	0.75 \pm 0.02	0.51 \pm 0.00	0.52 \pm 0.01	0.59 \pm 0.00	0.61 \pm 0.00	0.58 \pm 0.01	0.60 \pm 0.00	0.52 \pm 0.01	0.51 \pm 0.00
50	0.72 \pm 0.02	0.77 \pm 0.00	0.70 \pm 0.01	0.77 \pm 0.01	0.51 \pm 0.01	0.52 \pm 0.01	0.60 \pm 0.00	0.62 \pm 0.02	0.59 \pm 0.01	0.61 \pm 0.01	0.51 \pm 0.02	0.51 \pm 0.00
70	0.73 \pm 0.01	0.77 \pm 0.00	0.72 \pm 0.01	0.77 \pm 0.01	0.51 \pm 0.00	0.51 \pm 0.00	0.61 \pm 0.01	0.62 \pm 0.01	0.59 \pm 0.01	0.62 \pm 0.00	0.51 \pm 0.00	0.52 \pm 0.01

in this area (Kipf & Welling, 2016b): Area Under ROC Curve (AUC) and Average Precision (AP) scores. All the experiment results are averaged over 3 seeds.

Implementation details. We train the proposed model for 200 iterations using Adam. As for the mean and variance, we use 32-dimensional and 16-dimensional GCN layers to implement, respectively.

Main results. We benchmark all the methods across 6 real-world datasets. In Table 2, we observe that CCVGAE (ours) can reliably compete others with up to 29% improvement regarding AUC and 19% improvement regarding AP. Recall that CCVGAE improves on VGAE by integrating a causal layer to encourage disentangled representations, suggesting that the significant improvement is due to the expressiveness of those disentangled representations. SIG-VAE improve the representation by imposing graph structure-aware distributions instead of independent Gaussian, which results in better performance than VGAE. DGAE enhances VGAE by deepening GCN layers resulting in a better result than VGAE, especially for non-Euclidean data.

Additionally, we find that the performance on the Cora dataset shows different trends than other datasets. We hypothesize that such data could be generated under nearly independent factors, thus countering the validity of our assumption, i.e., $p^*(X) = \int_{Z^*} p^*(X|Z^*)p^*(Z^*)dZ^*$ with $p^*(Z^*) \neq \prod_i p(Z_i^*)$, and resulting in poor performance.

We also experiment on the synthetic data with a predefined causal structure and achieve advantages as before. In Figure 2(a), we present performance for all methods by varying the variance of ε in a large range: from 10 to 300. Interestingly, we find that the performance varies little as the noise level increases, implying that these VAE-based methods are

robust to noise as they capture the variance of the distribution well. Together, the robustness of our model benefits from the modeling of causality and variances.

6.2. Task 2: Few Shot Link Prediction

In this experiment, we aim to demonstrate the effectiveness of the proposed CC-Meta-Graph. As this is a meta-learning model, it consists of a meta-training phase followed by a testing phase, and its goal is to transfer knowledge from meta-training to the test phase. We will investigate the performance of all methods regarding (1) the number of meta-training loops and (2) the meta-training data requirement because these are the keys to a meta-learning model’s performance.

Baselines. Our experiment consists of three baselines corresponding to Meta-Graph (Bose et al., 2019) modifications, which employ pre-trained VGAEs, pre-trained CC-VGAEs, and randomness for initialization, called Meta-Graph, CC-Meta-Graph and Rand-Meta-Graph, respectively. In particular, the first baselines two are pre-trained on training graphs and fine-tuned on test graphs.

Datasets. We experiment on two benchmark datasets (Bose et al., 2019; Zitnik & Leskovec, 2017), including protein-protein interaction (PPI) and FirstMM DB. In this experiment, for all datasets, we perform link prediction by meta-training on a small subset of edges and then infer unseen edges. Under all settings, we use 80% of these graphs to pre-train weights and 10% as meta-validation, optimizing the global model parameters, and the rest for meta-testing. In terms of link prediction, we train all methods with two different settings: 5% and 10% edges of graphs, trying to see the effectiveness of using the data. Apart from meta-

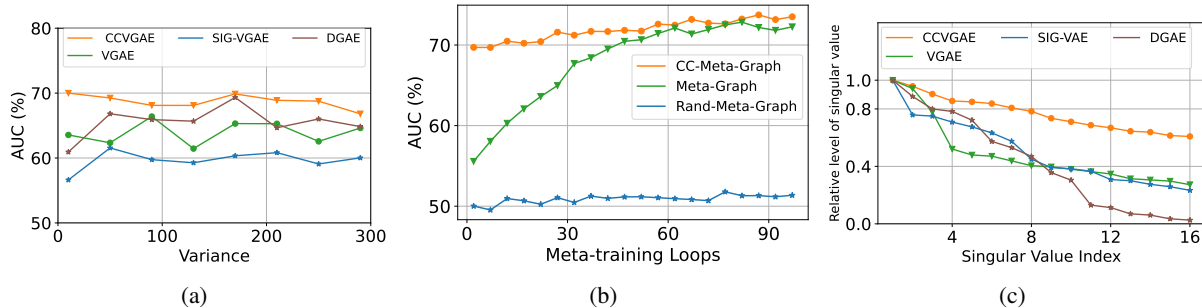


Figure 2. (a): The comparison of all baselines of the few shot link prediction task on the synthetic data set. The x-axis denotes the variance of ε , which is used to construct the synthetic dataset. The index of the maximum is 1, the smaller the value and the larger the index. (b): The performance of three methods when varying the number of meta-training loops (the PPI dataset). (c): The redundancy reduction analysis for causal disentangled representation. We take SVD of representations and normalize the eigenvalues to make the maximum as 1. The X-axis is the index of sorted normalized singular value, i.e., the first one denotes the largest value.

training, we always use 20% of edges for validation and the rest for testing.

Main results. In Table 3, we present the performance of all methods under different settings. Our method, CC-Meta-Graph, outperforms others consistently, providing up to a 11% absolute improvement. Notably, we can see that with 5% of the data, the performance of CC-Meta-Graph is competitive with the others given 10%, suggesting that our model can produce better generalizable representations with much less data and align with the consistency property.

We also evaluate how our model behaves under different meta-training epochs, as shown in Figure 2(b). Our method shows near-optimal performance even with only a few loops as opposed to a few dozen loops for Meta-Graph. Since Rand-Meta-Graph passes random values to the fine-tuning stage and thus can not benefit from the meta-training mechanism, resulting in the worst performance consistently.

To summarize, the superiority of our model validates the effectiveness of transferring global information to newly arrived data, even with significantly small data and only a few training loops, making our proposed method applicable under a limited budget.

6.3. Ablation Study

Module Importance. Recall that, for representation learning, we employ a causal structure to enforce disentanglement, which is DAG-structured Φ in Eq. 5. Thereby, we investigate how our method performs without such a causality structure constraint, called CCVGAE w/o CC. In Table 2, we find that the model without the DAG constraint, i.e., CCVGAE w/o CC, reduces the absolute performance by 12% and 12% regarding AUC and AP, respectively. These ablation results suggest the necessity of causal structure in our model.

The necessity of \mathcal{L}_{MSE} . We investigate how our method performs without \mathcal{L}_{MSE} , called CCVGAE w/o MSE. In table A.8, we find CCVGAE and CCVGAE w/o MSE have similar performance (within 2% absolute gap) in Corn, Texas, Actor. In Cora, dRisk, Wisconsin, CCVGAE w/o MSE reduces the absolute performance by up to 5% and 7% regarding AUC and AP, respectively. These results suggest that \mathcal{L}_{MSE} may slightly improve performance in some data, but not major.

6.4. Analysis on the redundancy reduction

We now present a redundancy reduction perspective to understand the effectiveness of our disentangled representations. In particular, we apply the singular value decomposition (SVD) on the obtained representations from Texas dataset and compare the magnitudes of their eigenvalues, i.e., the importance of each eigenvector. In Figure 2(c), we observe that the singular values of our method decrease slower, demonstrating that the importance of these eigenvectors is less concentrated. This implies that our representations are less redundant, making them more expressive under low-dimensional settings.

7. Conclusion

In this paper, we provide a tight upper bound for the approximation of the optimal solution in the VAE framework, together with a practical solution, called Concept-free Causal Disentanglement. We then propose an enhanced VGAE by a new causal disentanglement layer with the above idea, called CCVGAE. In addition, we discover the consistency of our derived concepts, which motivates us to develop a meta-learning model, called CC-Meta-Graph, aiming to transfer global information from limited data to new ones. Our experimental results show the effectiveness of both models in the link prediction task and the few-shot one.

References

- Bengio, Y., Courville, A., and Vincent, P. Representation learning: A review and new perspectives. *IEEE transactions on pattern analysis and machine intelligence*, 35(8): 1798–1828, 2013.
- Bose, A. J., Jain, A., Molino, P., and Hamilton, W. L. Meta-graph: Few shot link prediction via meta learning. *arXiv preprint arXiv:1912.09867*, 2019.
- Burgess, C. P., Higgins, I., Pal, A., Matthey, L., Watters, N., Desjardins, G., and Lerchner, A. Understanding disentangling in β -vae. *arXiv preprint arXiv:1804.03599*, 2018.
- Eastwood, C. and Williams, C. K. A framework for the quantitative evaluation of disentangled representations. In *International Conference on Learning Representations*, 2018.
- Fan, S., Wang, X., Mo, Y., Shi, C., and Tang, J. Debiasing graph neural networks via learning disentangled causal substructure. *arXiv preprint arXiv:2209.14107*, 2022.
- Hamilton, W. L. Graph representation learning. *Synthesis Lectures on Artificial Intelligence and Machine Learning*, 14(3):1–159, 2020.
- Hasanzadeh, A., Hajiramezani, E., Narayanan, K., Duffield, N., Zhou, M., and Qian, X. Semi-implicit graph variational auto-encoders. *Advances in neural information processing systems*, 32, 2019.
- Higgins, I., Matthey, L., Pal, A., Burgess, C., Glorot, X., Botvinick, M., Mohamed, S., and Lerchner, A. beta-vae: Learning basic visual concepts with a constrained variational framework. 2016.
- Higgins, I., Amos, D., Pfau, D., Racaniere, S., Matthey, L., Rezende, D., and Lerchner, A. Towards a definition of disentangled representations. *arXiv preprint arXiv:1812.02230*, 2018.
- Hoyer, P., Janzing, D., Mooij, J. M., Peters, J., and Schölkopf, B. Nonlinear causal discovery with additive noise models. *Advances in neural information processing systems*, 21, 2008.
- Jiang, W. and Luo, J. Graph neural network for traffic forecasting: A survey. *Expert Systems with Applications*, 207:117921, nov 2022.
- Joyce, J. M. Kullback-leibler divergence. In *International encyclopedia of statistical science*, pp. 720–722. Springer, 2011.
- Kim, H. and Mnih, A. Disentangling by factorising. In *International Conference on Machine Learning*, pp. 2649–2658. PMLR, 2018.
- Kipf, T. N. and Welling, M. Variational graph auto-encoders, 2016a. URL <https://arxiv.org/abs/1611.07308>.
- Kipf, T. N. and Welling, M. Variational graph auto-encoders. *arXiv preprint arXiv:1611.07308*, 2016b.
- Kocaoglu, M., Snyder, C., Dimakis, A. G., and Vishwanath, S. Causalgan: Learning causal implicit generative models with adversarial training. *arXiv preprint arXiv:1709.02023*, 2017.
- Krajewski, G. and Matthews, D. Rh baayen, analyzing linguistic data: A practical introduction to statistics using r. cambridge: Cambridge university press, 2008. pp. 368. isbn-13: 978-0-521-70918-7. *Journal of Child Language*, 37(2):465–470, 2010.
- Kumar, A., Sattigeri, P., and Balakrishnan, A. Variational inference of disentangled latent concepts from unlabeled observations. *arXiv preprint arXiv:1711.00848*, 2017.
- Li, Y. and Mandt, S. Disentangled sequential autoencoder. In *International Conference on Machine Learning*, 2018.
- Locatello, F., Bauer, S., Lucic, M., Raetsch, G., Gelly, S., Schölkopf, B., and Bachem, O. Challenging common assumptions in the unsupervised learning of disentangled representations. In *international conference on machine learning*, pp. 4114–4124. PMLR, 2019.
- Locatello, F., Bauer, S., Lucic, M., Ratsch, G., Gelly, S., Schölkopf, B., and Bachem, O. A commentary on the unsupervised learning of disentangled representations. In *Proceedings of the AAAI Conference on Artificial Intelligence*, volume 34, pp. 13681–13684, 2020.
- Ma, J., Cui, P., Kuang, K., Wang, X., and Zhu, W. Disentangled graph convolutional networks. In *International conference on machine learning*, pp. 4212–4221. PMLR, 2019.
- Paige, B., van de Meent, J.-W., Desmaison, A., Goodman, N., Kohli, P., Wood, F., Torr, P., et al. Learning disentangled representations with semi-supervised deep generative models. *Advances in neural information processing systems*, 30, 2017.
- Pei, H., Wei, B., Chang, K. C.-C., Lei, Y., and Yang, B. Geom-gcn: Geometric graph convolutional networks. *arXiv preprint arXiv:2002.05287*, 2020.
- Ping, H. Independence decomposition of multidimensional random variables. In *Proceedings of the 12th Annual Academic Conference of China Field Statistics Research Association*, 2005.
- Schölkopf, B. and von Kügelgen, J. From statistical to causal learning. *arXiv preprint arXiv:2204.00607*, 2022.

- Sen, P., Namata, G., Bilgic, M., Getoor, L., Galligher, B., and Eliassi-Rad, T. Collective classification in network data. *AI magazine*, 29(3):93–93, 2008.
- Shen, X., Liu, F., Dong, H., Lian, Q., Chen, Z., and Zhang, T. Weakly supervised disentangled generative causal representation learning. *Journal of Machine Learning Research*, 23:1–55, 2022.
- Shimizu, S., Hoyer, P. O., Hyvärinen, A., Kerminen, A., and Jordan, M. A linear non-gaussian acyclic model for causal discovery. *Journal of Machine Learning Research*, 7(10), 2006.
- Suter, R., Miladinovic, D., Schölkopf, B., and Bauer, S. Robustly disentangled causal mechanisms: Validating deep representations for interventional robustness. In *International Conference on Machine Learning*, pp. 6056–6065. PMLR, 2019.
- Tang, J., Sun, J., Wang, C., and Yang, Z. Social influence analysis in large-scale networks. In *Proceedings of the 15th ACM SIGKDD international conference on Knowledge discovery and data mining*, pp. 807–816, 2009.
- Trauble, F., Creager, E., Kilbertus, N., Locatello, F., Dittadi, A., Goyal, A., Schölkopf, B., and Bauer, S. On disentangled representations learned from correlated data. In *International Conference on Machine Learning*, 2020.
- Träuble, F., Creager, E., Kilbertus, N., Locatello, F., Dittadi, A., Goyal, A., Schölkopf, B., and Bauer, S. On disentangled representations learned from correlated data. In *International Conference on Machine Learning*, pp. 10401–10412. PMLR, 2021.
- Wu, S., Sun, F., Zhang, W., Xie, X., and Cui, B. Graph neural networks in recommender systems: A survey, 2020. URL <https://arxiv.org/abs/2011.02260>.
- Wu, X. and Cheng, Q. Stabilizing and enhancing link prediction through deepened graph auto-encoders. In *IJCAI: proceedings of the conference*, volume 2022, pp. 3587–3593. NIH Public Access, 2022.
- Xu, R., Li, L., and Wang, Q. driskkb: a large-scale disease-disease risk relationship knowledge base constructed from biomedical text. *BMC bioinformatics*, 15(1):1–13, 2014.
- Yang, M., Liu, F., Chen, Z., Shen, X., Hao, J., and Wang, J. Causalvae: Disentangled representation learning via neural structural causal models. In *Proceedings of the IEEE/CVF Conference on Computer Vision and Pattern Recognition*, pp. 9593–9602, 2021.
- Yang, Y., Feng, Z., Song, M., and Wang, X. Factorizable graph convolutional networks. *Advances in Neural Information Processing Systems*, 33:20286–20296, 2020.
- You, J., Liu, B., Ying, R., Pande, V., and Leskovec, J. Graph convolutional policy network for goal-directed molecular graph generation. In *Proceedings of the 32nd International Conference on Neural Information Processing Systems, NIPS’18*, pp. 6412–6422, Red Hook, NY, USA, 2018. Curran Associates Inc.
- Yu, Y., Chen, J., Gao, T., and Yu, M. Dag-gnn: Dag structure learning with graph neural networks. In *International Conference on Machine Learning*, pp. 7154–7163. PMLR, 2019.
- Zhang, K. and Hyvarinen, A. On the identifiability of the post-nonlinear causal model. *arXiv preprint arXiv:1205.2599*, 2012.
- Zhang, S., Tong, H., Xu, J., and Maciejewski, R. Graph convolutional networks: Algorithms, applications and open challenges. In *Computational Data and Social Networks: 7th International Conference, CSoNet 2018, Shanghai, China, December 18–20, 2018, Proceedings 7*, pp. 79–91. Springer, 2018.
- Zhou, J., Cui, G., Hu, S., Zhang, Z., Yang, C., Liu, Z., Wang, L., Li, C., and Sun, M. Graph neural networks: A review of methods and applications. *AI Open*, 1:57–81, 2020.
- Zhu, X., Xu, C., and Tao, D. Commutative lie group vae for disentanglement learning. In *International Conference on Machine Learning*, pp. 12924–12934. PMLR, 2021.
- Zitnik, M. and Leskovec, J. Predicting multicellular function through multi-layer tissue networks. *Bioinformatics*, 33(14):i190–i198, 2017.

A. Appendix

A.1. Proof of Theorem 4.1

Before detailing the proof, we first introduce two necessary lemmas.

Lemma 1. $\forall K$ dimension continuous variable $X = (X_1, \dots, X_K)$, if the support set of its joint probability density is a convex set in R^K , then $\exists K$ dimensional independent uniform variables $U = (U_1, \dots, U_K)$ and a set of function $F = \{f_1, f_2, \dots, f_K\}$ result in $X = F(U)$ that $X_k = f_k(U_1, \dots, U_k)$.

The proof of Lemma 1 is provided by [Ping \(2005\)](#). The above lemma indicates that it is possible to represent continuous observations with convex joint density distributions by projecting a list of independent variables onto some functions. We now present the following lemma showing that any given continuous variable can be associated with a uniform distribution.

Lemma 2. \forall continuous variable X , set its distribution function as $f(X) = P(X \leq x)$, then $f(X) \sim U(0, 1)$.

Proof. $P(f(X) \leq a) = P(X \leq f^{-1}(a)) = f(f^{-1}(a)) = a$, where a is a constant. \square

Then we prove Theorem 4.1:

Proof. Generally, proving Theorem 4.1 is equal to finding functions $q_i, i = 1, 2, \dots, K$ that make $G_i = q_i(N_i^S) = Z_i^*, N^S \subseteq N$ true. We now present the proof in four steps as follows.

Step 1: Because of Lemma1, we get that there exists independent uniform variables (U_1, \dots, U_K) and function F make $Z^* = F(U)$, in which:

$$U = (U_1, \dots, U_K) \quad (8)$$

$$Z_i^* = f_i(U_1, \dots, U_i) \quad (9)$$

Set $U_i \sim U(a_i, b_i), i = 1, 2, \dots, K$.

Step 2: Set there are arbitrary K independent normal variables $N_1, \dots, N_K, N_i \sim N(\mu_i, \sigma_i^2)$. Set distribution function of N_i is g_i , which means $g_i(x) = P(N_i \leq x)$. Denote:

$$g_i(N_i) = U'_i, i = 1, 2, \dots, K \quad (10)$$

Step 3: Because of Lemma2, U'_1, \dots, U'_K are independent and they all are variables of uniform distribution $U(0, 1)$.

Then U_i in Step 1 can be represents by U'_i as:

$$U_i = (b_i - a_i)U'_i + a_i, i = 1, 2, \dots, K \quad (11)$$

Because $g_i(N_i) = U'_i$ in (10), which means U'_i is function of N_i , so we can denote:

$$(b_i - a_i)U'_i + a_i = (b_i - a_i)g_i(N_i) + a_i = h_i(N_i) \quad (12)$$

Step 4: Then we can find $Z_i^* = q_i(N_1, \dots, N_i)$ as:

$$Z_i^* = f_i(h_1(N_1), h_2(N_2), \dots, h_i(N_i)) = q_i(N_1, \dots, N_i) \quad (13)$$

In which set of f_i is from equation 9 and h_i is from equation 12. Therefore, we can induce Theorem 4.1 is right because $\forall Z^*$ (in equation $p^*(X) = \int_{Z^*} p^*(X|Z^*)p^*(Z^*)dZ^*$), \exists a function Q makes $G = Q(N^S) = \{q_i(N_1, \dots, N_i)\}_{i=1,2,\dots,K}$ (from equation (13)) is equal to Z^* . \square

A.2. Proof of Proposition 1

Proof.

Let A as a lower triangular matrix, \hat{A} is permuted from A . We can induce that $\hat{A} * \text{diag}(N)$ can be acquired by such matrix with finite row exchange :

$$\begin{pmatrix} A_{11}N_1 & 0 & 0 & \dots & 0 \\ A_{21}N_1 & A_{22}N_2 & 0 & \dots & 0 \\ A_{31}N_1 & A_{32}N_2 & A_{33}N_3 & \dots & 0 \\ \dots & \dots & \dots & \dots & \dots \\ A_{K1}N_1 & A_{K2}N_2 & A_{K3}N_3 & \dots & A_{KK}N_K \end{pmatrix}$$

Where $\hat{A} = \{A_{ij}\}$. So we can induce that for each q_i in Equation 13, there must exist one row of $\hat{A} * \text{diag}(N)$ equal to $(a_{i1}N_1, a_{i2}N_2, \dots, a_{ii}N_i)$, which is exactly $q_i^{-1}(Z_i^*)$. So optimal generative factors $G = Z^*$ can be expressed as $\hat{A} * \text{diag}(N)$. \square

Now we provide a remark that implies any functions Q' with the mentioned two conditions is guaranteed to meet the same mapping relationships with the true function Q , which makes G' acquired by such Q has the same statistical properties with the true G .

Remark 1. Consider a function set $Q' = \{Q'_1, \dots, Q'_K\}$ that computes causal generative factors with a row-wise formulation as $G_i = Q'_i(B_i)$. Assuming $B = A * \text{diag}(N') \in \mathbb{R}^{K \times K}$, along with the following conditions:

Condition 1: $A \in \mathbb{R}^{K \times K}$ can be obtained by finite row exchanges of a lower triangular matrix;

Condition 2: N' consists of K independent normal variables as $N' = (N'_1, N'_2, \dots, N'_K)^T$;

then

(1) There must exist two real numbers denoted as a_i and b_i , and exist $N_k \in N$ as in Theorem 4.1, such that the following equation holds: $N'_i = a_i \times N_k + b_i, i = 1, 2, \dots, K$.

(2) Denote $Q = \{Q_1, Q_2, \dots, Q_K\}$ (in Theorem 4.1) and $Q_i^{-1}(G_i) = N_i^S \subseteq \{N_1, N_2, \dots, N_K\}$, then for each Q_i there must exist $Q'_m \in Q'$ and a constant diagonal matrix V_i and constant vector M_i such that: $Q_i^{-1}(G_i) = V_i Q'_m{}^{-1}(G_i) + M_i = N_i^S$ if Q_i and Q'_m are reversible.

Proof. Proof of Remark 1 is equal to proving such 2 statements:

(1) $\forall i$ in $1, 2, \dots, K$, there exist a constant diagonal matrix V_i and constant vector M_i that $N_i^{S'} = (N'_1, N'_2, \dots, N'_i)$ can be acquired by $N_i^S = (N_1, N_2, \dots, N_i)$: $N_i^{S'} = V_i N_i^S + M_i$.

(2) $Q = \{q_1, q_2, \dots, q_K\}$ in Equation 13 is unique.

Proof of statement(1):

Because \forall two normal variables with the same dimensions, denoting N_i and N'_i , there exist two constant v_i, m_i that $N'_i = v_i N_i + m_i$. Statement(2) just represents $N'_i = v_i N_i + m_i$ as random vector.

Proof of statement(2):

Because f_i and h_i is unique. So q_i is unique and Q is unique. \square

The (1) in Theorem 1 can be acquired by statement(1). Because statement(2) tells us Q is unique, so we can induce by Proposition 1 that Equation 13 can also be acquired by $G_i = Q_i(B_i) = Q'_i(B_i)$ if $N = N'$. However, we can not ensure $N = N'$, so with statement(2), we can induce (2) in Theorem 1.

A.3. Proof of Theorem 4.2

Before proof, we need a lemma as following:

Lemma 3. Denote the distribution function of normal variable $N \sim (\mu, \sigma^2)$ as $F_N(x)$. There exist a linear function $f_L(x)$: (1) Make the absolute error $|F_N(x) - f_L(x)| \leq \frac{1}{\sqrt{2\pi}}x(1 - e^{-\frac{x^2}{2\sigma^2}})$ (2) If $x \in [\mu - \varepsilon, \mu + \varepsilon]$, then the absolute error $|F_N(x) - f_L(x)| \leq \frac{1}{\sqrt{2\pi}}\varepsilon(1 - e^{-\frac{\varepsilon^2}{2\sigma^2}})$

Proof. The proof of (1): Without losing generalization, we consider $\mu = 0$ and the linear function is $f_L(x) = \frac{1}{\sqrt{2\pi}}x + \frac{1}{2}$. We only consider $x > 0$, because both of $f_L(x)$ and distribution function are central symmetric about $(0, \frac{1}{2})$, so

the absolute error is same when $x < 0$.

$$\begin{aligned}
 & |F_N(t) - f_L(t)| \\
 &= \left(\frac{1}{\sqrt{2\pi}}t + \frac{1}{2}\right) - \int_{-\infty}^t \frac{1}{\sqrt{2\pi}}e^{-\frac{x^2}{2\sigma^2}} dx \\
 &= \frac{1}{\sqrt{2\pi}}t - \int_0^t \frac{1}{\sqrt{2\pi}}e^{-\frac{x^2}{2\sigma^2}} dx \\
 &= \int_0^t \frac{1}{\sqrt{2\pi}} dx - \int_0^t \frac{1}{\sqrt{2\pi}}e^{-\frac{x^2}{2\sigma^2}} dx \\
 &= \int_0^t \frac{1}{\sqrt{2\pi}}(1 - e^{-\frac{x^2}{2\sigma^2}}) dx \\
 &\leq \int_0^t \frac{1}{\sqrt{2\pi}}(1 - e^{-\frac{t^2}{2\sigma^2}}) dx \\
 &= \frac{1}{\sqrt{2\pi}}t(1 - e^{-\frac{t^2}{2\sigma^2}})
 \end{aligned} \tag{14}$$

The proof of (2): Without losing generalization, we consider $\mu = 0$. Because $\frac{1}{\sqrt{2\pi}}t(1 - e^{-\frac{t^2}{2\sigma^2}})$ is a increasing function. If $t \in [0, \varepsilon]$, $\frac{1}{\sqrt{2\pi}}t(1 - e^{-\frac{t^2}{2\sigma^2}}) \leq \frac{1}{\sqrt{2\pi}}\varepsilon(1 - e^{-\frac{\varepsilon^2}{2\sigma^2}})$. The same as $t \in [-\varepsilon, 0]$. \square

Now we prove Theorem 4.2:

Proof. Assume $Z_1^*, Z_2^*, \dots, Z_K^*$ is a linear uniform distribution means that: $P(Z_1^*) \sim U(\eta_1 + r_{10}, \eta_1 + r_{11})$ and $P(Z_k^* | Z_1^*, \dots, Z_{k-1}^*) \sim U(\eta_k + r_{k0}, \eta_k + r_{k1}), k = 2, \dots, K$ with $\eta_k = \sum_{t=1}^{k-1} \omega_{kt} Z_t^*$, and $\omega_{k1}, \omega_{k2}, \dots, \omega_{k(k-1)}, r_{k0}, r_{k1}$ is real number. Then we can get that the conditional distribution when Z_k^* is in its non-zero interval:

$$\begin{aligned}
 & P(Z_k^* \leq z_k^* | Z_1^* = z_1^*, Z_2^* = z_2^*, \dots, Z_{k-1}^* = z_{k-1}^*) \\
 &= \frac{1}{r_{k1} - r_{k0}}(z_k^* - r_{k0}) + \omega_{k1}z_1^* + \dots + \omega_{k(k-1)}z_{k-1}^*
 \end{aligned} \tag{15}$$

We can find that this conditional distribution is a linear function of (z_1^*, \dots, z_k^*) . Moreover, we can induce by Mathematical Induction that the joint distribution $P(Z_1^*, \dots, Z_k^*) = P(Z_k^* | Z_1^*, \dots, Z_{k-1}^*)P(Z_1^*, \dots, Z_{k-1}^*)$ is a constant when (Z_1^*, \dots, Z_k^*) is in their non-zero interval.

We can find the formulation of f_i in Lemma 1 in Ping (2005) as:

$$f_i(x_1, x_2, \dots, x_k) = \frac{p_X(X_i \leq x_i | X_1 = x_1, X_2 = x_2, \dots, X_{i-1} = x_{i-1})}{p_X(x_1, \dots, x_{k-1})}$$

p_X means the probability dense function of X in Lemma 1, but in equation 9, p_X means the dense function of $Z^* = \{Z_1^*, Z_2^*, \dots, Z_K^*\}$ in true data set. So we can induce from equation 15 that, the numerator of $f_i(U_1, \dots, U_i)$ in equation 9 is linear function of U_1, \dots, U_i and denominator is

a constant. Therefore, equation 9 is a linear function of U_1, \dots, U_i , denoting as:

$$\begin{aligned} f_i(U_1, \dots, U_i) \\ = \rho_{i0} + \rho_{i1}U_1 + \dots + \rho_{i(i-1)}U_{i-1} + \rho_{ii}U_i \end{aligned} \quad (16)$$

In equation 13, h_i is $(b_i - a_i)g_i(N_i) + a_i$, where g_i is the distribution of normal variable. Without losing generality, we set $b_i = 1, a_i = 0$, then we have $h_i = g_i$, which has the absolute error bound with a linear function as Lemma 3. Based on equation 16 and Lemma 3, we can get there exist a linear function $f_L(N_1, N_2, \dots, N_i) = \sum_{k=1}^i f_{Lk}(N_k)$ has the bound with and the optimal solution $G = Z_i^*$ when $N_i \in [\mu_i - \delta, \mu_i + \delta]$ because:

$$\begin{aligned} & |f_i(h_1(N_1), h_2(N_2), \dots, h_i(N_i)) - f_L(N_1, N_2, \dots, N_i)| \\ & = |\rho_{i0} + \rho_{i1}h_1(N_1) + \dots + \rho_{i(i-1)}h_{i-1}(N_{i-1}) + \rho_{ii}h_i(N_i) \\ & \quad - \sum_{k=1}^i f_{Lk}(N_k)| \\ & \leq |\sum_{k=1}^i (\rho_{ik}h_1(N_k) - f_{Lk}(N_k))| + |\rho_{i0}| \\ & \leq |\rho_{i0}| + \frac{\delta}{\sqrt{2\pi}} \sum_{k=1}^i \rho_{ik} (1 - e^{-\frac{\delta^2}{2\sigma_k^2}}) \\ & = |\rho_{i0}| + \delta (\sum_{k=1}^i \frac{\rho_{ik}}{\sqrt{2\pi}} - \sum_{k=1}^i \frac{\rho_{ik}}{\sqrt{2\pi}} e^{-\frac{\delta^2}{2\sigma_k^2}}) \\ & = |\rho_{i0}| + \delta (\sum_{k=1}^i \frac{\rho_{ik}}{\sqrt{2\pi}} - \sum_{k=1}^i \frac{\rho_{ik}}{\sqrt{2\pi}} (e^{-\frac{1}{2\sigma_k^2}})^{\delta^2}) \\ & = a_i + \delta (b_i + \sum_{k=1}^i c_{ik} d_k^{\delta^2}) \end{aligned} \quad (17)$$

□

A.4. Proof of Proposition 2

Proof. Now we start from one of rows in $\hat{A} * \text{diag}(N')$ which is $(a_{i1}N_1, a_{i2}N_2, a_{i3}N_3, 0, \dots, 0)$ (for simplicity, we denote this row is i -th row. Note that there must exist such a row because \hat{A} is permuted from triangular matrix). In Theorem 4.2, we proved that Q' can be implemented as a linear function. So $G'_i = Q'_i(B_i) = Q'_i(\{\hat{A} * \text{diag}(N')\}_i) = Q'_i(a_{i1}N_1, a_{i2}N_2, a_{i3}N_3, 0, \dots, 0)$. So:

$$\begin{aligned} & Q'_i(a_{i1}N_1, a_{i2}N_2, a_{i3}N_3, 0, \dots, 0) \\ & = q_{i1}a_{i1} * N_1 + q_{i2}a_{i1} * N_2 + q_{i3}a_{i1} * N_3 \\ & = (q_{i1}a_{i1}, q_{i2}a_{i2}, q_{i3}a_{i3}, 0, \dots, 0) * (N_1, N_2, N_3, \dots, N_K)^T \\ & \longrightarrow (c_{i1}, c_{i2}, c_{i3}, 0, \dots, 0) * (N_1, N_2, N_3, \dots, N_K)^T \\ & = \tilde{A}_i * N' \end{aligned} \quad (18)$$

Here $\tilde{A}_i = (c_{i1}, c_{i2}, c_{i3}, 0, \dots, 0)$ and $N' = (N_1, N_2, N_3, \dots, N_K)^T$. We can adopt this expression method to other rows. Finally, we can make such conclusion: \hat{A} is a matrix with the same non-zero position as \tilde{A} , means that \hat{A} is also a matrix permuted from lower triangular matrix. □

A.5. Formal version of Theorem 4.3

Given n observations $\{X^{(1)}, X^{(2)}, \dots, X^{(n)}\}$ sampled from the same distribution $p^*(X)$, along with their corresponding optimal generative factors $\{Z^{(1)}, Z^{(2)}, \dots, Z^{(n)}\}$, a function $Z^{(n)}$ with these generative factors will converge to the same ground truth (GT) concept \check{Z} as $\lim_{n \rightarrow \infty} Z^{(n)} = \check{Z}$, where $Z^{(n)} = (Z^{(1)} + Z^{(2)} + \dots + Z^{(n)})/n$.

Proof. The conclusion can be easily deduced from the law of large numbers. □

A.6. Proof of $(I - \Phi^T)^{-1}$

Before the proof, we need a lemma:

Lemma 4. *If D is the adjacency matrix of DAG with nodes vector Z , which means that $Z = DZ$. Then there exist a lower triangular matrix T and a vector Z' acquired by finite row exchange of Z , making $Z' = TZ'$.*

Proof. In a DAG, there must exist at least one node with 0 in-degree. We can remove arbitrary one node with 0 in-degree, and make this node as the first node in Z' .

Because the graph without this node is also a DAG, so we can also find at least one node with 0 in-degree, and make the second node in Z' . Because the second node's in-degree is 0 in graph without the first node, so the first line of T has at most 1 non-zero element.

Repeat this process and we can find such T and Z' . □

To prove the $(I - \Phi^T)^{-1}$ can be acquired by a lower triangular matrix with finite row exchange, we need to prove:

There exist a lower triangular matrix L and a elementary matrix $P_{K \times K}$ acquired by unit matrix with finite row exchange, making that $G^T = (I - \Phi^T)^{-1} \epsilon^T = PL\epsilon^T$, Φ is DAG adjacency matrix with nodes vector G^T .

Now we have such proof:

Proof. With Lemma 4, we can induce that there exist a lower triangular matrix T and a vector G_R^T acquired by finite row exchange of G^T , making $G_R^T = TG_R^T + \epsilon \rightarrow G_R^T = (I - T)^{-1}\epsilon^T$.

Because G_R^T is acquired by finite row exchange of G^T , we can denote $G_R^T = P'G^T$, P' is acquired by unit matrix with finite row exchange. So we have $P'G^T = (I - T)^{-1}\epsilon^T \rightarrow G^T = P'^{-1}(I - T)^{-1}\epsilon^T$. Let $P = P'^{-1}$, $L = (I - T)^{-1}$, then we have $G^T = PL\epsilon^T$. \square

A.7. Algorithm of CCVGAE and Causal-Meta-Graph for Few Shot Link Prediction

Algorithm 1: Concept-free Causal-Meta-Graph for Few Shot Link Prediction

Result: GNN global parameters ϕ , Graph signature function ψ , Global causal layer parameters C

Initialize learning rates: α, β, γ ;

Sample a mini-batch of graphs, G_{batch} from $p(G)$

for each $G \in G_{batch}$ **do**

$\epsilon = \epsilon^{train} \cup \epsilon^{val} \cup \epsilon^{test}$ // Split edges into train, val, and test;;

$s_G = \psi(G, \epsilon^{train})$ // Compute graph signature;

Initialize: $\phi(0) \leftarrow \phi$ // Initialize local parameters via global parameters

for k in $[1 : K]$ **do**

$s_G = stopgrad(s_G)$ // Stop Gradients to Graph Signature;

$Z = (I - C^T)^{-1}s_G$ // Compute hidden representation;

$L_{train} = -ELBO_{train} + \alpha H(C)$;

Update $\phi(k) \leftarrow \phi(k - 1) - \beta \nabla \phi L_{train}$

end

Initialize: $\phi \leftarrow \phi_K$;

$s_G = \psi(G, \epsilon_{val} \cup \epsilon_{train})$ // Compute graph signature with validation edges;

$L_{val} = -ELBO_{val} + \alpha H(C)$;

Update $\phi \leftarrow \phi - \gamma \nabla \phi L_{val}$;

Update $\psi \leftarrow \psi - \gamma \nabla \psi L_{val}$;

Update $C \leftarrow C - \gamma \nabla C L_{val}$

end

A.8. Ablation study result

Algorithm 2: CCVGAE

Input: Graph edges \mathcal{E} , node features X , α, β

Initialize GCN parameters GCN_μ, GCN_σ , causal matrix Φ ;

$\mathcal{E} = \mathcal{E}^{train} \cup \mathcal{E}^{val} \cup \mathcal{E}^{test}$ // Split edges into train, val, and test;

$A = A_{train} + A_{val} + A_{test}$ // Generate train, valid, test adjacency

for $epoch$ in $[1 : number\ of\ epoch]$ **do**

$\mu = GCN_\mu(A_{train}, X)$ // Compute mean of ϵ ;

$\sigma = GCN_\sigma(A_{train}, X)$ // Compute variance of ϵ ;

$\epsilon = N(\mu, \sigma)$ // Generate ϵ as independent normal distribution;

$G = (I - C^T)^{-1}\epsilon$ // Compute generate factors;

$\hat{A}_{train} = \sigma_1(G_i^T \hat{G}_j)$ // Reconstruct adjacency matrix;

$\hat{X} = \sigma_2(G)$ // Reconstruct node features;

$\mathcal{L}_{train} = -\mathcal{L}_G + \alpha \mathcal{L}_\Phi + \beta \mathcal{L}_{MSE}$;

Update $GCN_\mu, GCN_\sigma, \Phi$

end

Compute $ROC(A_{test}, \hat{A}_{test})$ and $AP(A_{test}, \hat{A}_{test})$

Table 4. AUC (%) and AP (%) scores for CCVGAE w/o MSE and CCVGAE on real-world datasets.

	CCVGAE w/o MSE		CCVGAE	
	AUC	AP	AUC	AP
Cora	0.80 \pm 0.02	0.82 \pm 0.03	0.85 \pm 0.03	0.85 \pm 0.05
Corn	0.73 \pm 0.03	0.79 \pm 0.06	0.74 \pm 0.06	0.78 \pm 0.04
Texas	0.76 \pm 0.04	0.78 \pm 0.03	0.75 \pm 0.07	0.80 \pm 0.07
Wisconsin	0.72 \pm 0.07	0.77 \pm 0.06	0.75 \pm 0.04	0.79 \pm 0.05
dRisk	0.71 \pm 0.05	0.65 \pm 0.07	0.75 \pm 0.06	0.72 \pm 0.05
Actor	0.79 \pm 0.04	0.81 \pm 0.03	0.78 \pm 0.07	0.81 \pm 0.06